



First-principles study of water decomposition and hydrogen evolution on MgZn₂ Laves phase

Yaowei Wang^a, Tian Xie^b, Zhe Luo^b, Hong Zhu^{a,*}, Xiaoqin Zeng^{b,*}

^a University of Michigan - Shanghai Jiao Tong University Joint Institute, Shanghai Jiao Tong University, 200240 Shanghai, PRC, China

^b National Engineering Research Center of Light Alloy Net Forming, Shanghai Jiao Tong University, Shanghai 200240, PRC, China

ARTICLE INFO

Keywords:

Mg–Zn alloy
Corrosion
Hydrogen evolution reaction
First-principles calculations

ABSTRACT

Second phase strengthening has been widely applied in Mg alloy designs, many of which however have been reported to aggravate the galvanic corrosion of Mg alloys. In this study, the hydrogen evolution reaction (HER) on MgZn₂ Laves phase, which serves as a local cathode, is investigated by first-principles calculations based on density functional theories. We first calculated the surface energy of MgZn₂ and found (0001) surface with Mg-rich termination to be the most stable one, and the favored adsorption sites for relevant molecule species were further identified. By using Nudged Elastic Band (NEB) method, the reaction pathway and energy barriers of H₂O molecule decomposition, H adatom diffusion, and H₂ molecule recombination were obtained, among which hydrogen recombination is thermodynamically unfavored. This study provides fundamental insights into the cathodic reaction on Mg alloys, from determining the cathode, identifying the most stable surface, obtaining reaction energy barrier, to comparing corrosion property among different intermetallics, which may be a guidance to the corrosion-resistant Mg alloys design.

1. Introduction

Nowadays, nearly 20% carbon dioxide (CO₂) emissions are from burning fossil fuels for ground, air, and marine transportation [1,2], where the application of lightweight alloys with enhanced mechanical properties is beneficial. Magnesium (Mg) alloys are promising engineering metals in the aerospace and automotive industries due to their high specific strength (ratio of tensile strength to density). However, the poor corrosion resistance limits their further applications [3–8], to which much efforts should be devoted. It has been reported that alloying is an effective method to improve both mechanical and corrosion properties of magnesium alloys [9–11].

Up to now, some commercial magnesium alloys Mg-X (X = Al, Zn, Zr, RE) have been developed. Al is the most common addition to improve the strength of Mg because of low price [12]. AZ31 is believed to give an optimum balance between strength and corrosion properties for Mg alloys. Zr is added to Mg due to its ability to refine the grain size, improving both mechanical and casting properties [13]. Other rare earth elements, such as La, Y, Er and Ce are reported to modify the microstructure and enhance the protective effectiveness of surface oxide [14–16]. Among them, Mg-Zn alloy aroused great interests as promising

alternatives to permanent implant materials [17–19]. Zinc is an essential trace element for the human body and many experimental results revealed that the addition of Zn plays a very important role in refining grains and improving the corrosion resistance of Mg alloys [18,20,21]. Up to now, several Mg-Zn alloy systems have been studied, such as the Mg–Zn [22] binary system and Mg–Zn–RE [23,24] ternary system.

Mg-Zn alloys are one of the well-known ZK series of precipitation-hardening alloys with the fine and rod-like precipitated binary β_1 phase, which hinders the motion of dislocations and resists the basal slip. Some recent experiments on Mg-Zn and Mg-Zn-X (X = Ca, Zr, Ag) alloys showed that rod-like binary β_1 phase has a Laves MgZn₂ structure [25,26]. Therefore, understanding the fundamental mechanism of corrosion process on MgZn₂ is crucial for improving the corrosion resistance of Mg-Zn alloys. Yao et al. [27] measured polarization curves for pure Zn and Zn-Mg binary alloy and found that with the increase of Mg content the current density and corrosion potential do not change monotonously. Zhang et al. [28] and Birbilis et al. [29] reported that the corrosion potential of MgZn₂ is –1.03 V relative to the Saturated Calomel Electrode (SCE, a reference electrode based on the reaction between elemental mercury and mercury chloride), which indicated MgZn₂ would serve as the local cathode during the galvanic corrosion

* Corresponding authors.

E-mail addresses: hong.zhu@sjtu.edu.cn (H. Zhu), xqzeng@sjtu.edu.cn (X. Zeng).

process of Mg-Zn alloys. Recently, some density functional theory (DFT) studies of MgZn₂ have been performed, but not much on its corrosion-related properties. Shao et al. [30] calculated defect formation energy in MgZn₂. Mao et al. [31] and Wu et al. [32] had studied the stabilities and elastic properties of some common Mg intermetallics, systematically summarizing the elastic constants, bulk moduli, shear moduli and Poisson's ratio of MgZn₂, MgCu₂ and Mg₂Ca. Tsuru et al. [33] investigated the hydrogen segregation at the MgZn₂ precipitate in Al-Mg-Zn alloys, and the calculated trap energy elucidates that hydrogen tends to gather at the interface between MgZn₂ and Al.

On the other hand, some previous studies have devoted to hydrogen evolution reaction (HER) and water dissociation reaction on Mg(0001) surface [34–40], while limited investigations on the intermetallic phases are available. Considering the second phases and impurities in Mg alloys usually serve as the local cathode [41], a comprehensive theoretical investigation of the cathodic reaction on second phase surface, e.g., the reaction path and the associated energy barrier, is necessary to understand the reaction mechanisms of galvanic corrosion for Mg binary alloys.

In this work, we have applied the DFT calculations to theoretically study the galvanic corrosion behavior of Mg-Zn alloy, which is composed of Mg matrix and MgZn₂ intermetallic phase. According to the calculated equilibrium potential, MgZn₂ is determined to serve as the local cathode. The thermodynamics of the water dissociation, hydrogen adatom diffusion and hydrogen evolution reaction on the most stable MgZn₂ surface have been investigated by Nudged Elastic Band (NEB) method, where the rate-determining step for HER on MgZn₂ has been identified. Finally, the activation energy barrier of cathodic reactions on Mg, MgZn₂ and Mg₂Ge were compared and free energy of H adatom were suggested to be a quick criterion for screening the promising corrosion resistant Mg intermetallics.

2. Computational details

All DFT [42] calculations were carried out by using the projector augmented wave (PAW) [43] method, as implemented in the Vienna Ab Initio Simulation Package (VASP) [44]. The Perdew-Burke-Ernzerhof [45] version of the generalized gradient approximation (GGA) [46] is applied to describe the exchange–correlation energy functional. The cut-off energy of plane wave is set at 520 eV and the Brillouin zone integration uses Gamma-centered grids of 5 × 5 × 3 *k*-point mesh. The convergence criteria of energy and force are set to 10^{−6} eV/atom and 0.01 eV/Å, respectively. The optimized lattice parameters of MgZn₂ are *a* = 5.23 Å and *c* = 8.54 Å, in accordance with the experimental value (*a* = 5.20 Å and *c* = 8.57 Å [23,47,48]) and other theoretical results [30,49] (*a* = 5.22 Å and *c* = 8.57 Å). To study the cathodic reactions on MgZn₂ surface, a 2 × 2 supercell model with 15 Å vacuum layer was employed along *Z* direction, which is adequate to avoid the interaction between the repeating slabs. The (10 $\bar{1}$ 0), (11 $\bar{2}$ 0) and (0001) symmetric surfaces with different terminations have been considered in this work. The details about the surface models could be found in Fig. S1 of Supporting Information. During the process of surface optimizing, all the atoms in the slab are relaxed and no surface reconstruction is observed.

3. Results and discussion

3.1. Equilibrium potential and work function

Since Mg alloys are prone to the galvanic corrosion, it is necessary to determine the local anode and cathode [50,51]. In experiments, we usually identify the anode and cathode based on corrosion potential and most intermetallics will serve as the local cathode besides Mg₂Ca [29,41]. However, developing the corrosion-resistant Mg alloy based on experimental results is pretty hard due to the limited data. Our prior study proposed a positive correlation between the experimental

corrosion potential and the equilibrium potential which can be used as a quick criteria to determine the local cathode [52].

For pure Mg, the dissolution reaction is Mg → Mg²⁺ + 2e[−]. From Nernst equation, we can get the equilibrium potential of pure Mg

$$E(\text{Mg}|\text{Mg}^{2+}) = E^\circ(\text{Mg}|\text{Mg}^{2+}) + \frac{RT}{2F} \ln [c(\text{Mg}^{2+})] \quad (1)$$

where $E^\circ(\text{Mg}|\text{Mg}^{2+})$ is the standard potential of Mg, −2.37 V relative to the Standard Hydrogen Electrode (SHE, the primary reference electrode and declared to be 0 at standard state) [7]. $c(\text{Mg}^{2+})$ is the concentration of Mg²⁺, *R* is the universal gas constant, 8.314 K^{−1} mol^{−1}, *T* is the room temperature, 298 K, and *F* is the Faraday constant, 96485 C/mol. By convention, corrosion is considered to have happened when the minimum concentration of the dissolved ion reaches 10^{−6} mol/L [53], which has been applied for our equilibrium potential calculations in this work and the corresponding equilibrium potential of Mg is thus quantified to be −2.55 V_{SHE}.

Similarly, based on the DFT calculations and Nernst equation, we can derive the equilibrium potential of the intermetallic MgZn₂. From the pourbaix diagram [54,55], we assume the dissolution reaction accompanied by hydrogen evolution occurs in a neutral environment with all ionic concentration of 10^{−6} mol/L. Without over potential, the stable product MgZn₂ dissolution is Mg²⁺ and Zn²⁺. The corresponding reaction is MgZn₂ → Mg²⁺ + 2Zn²⁺ + 6e[−] and the equilibrium potential of MgZn₂ can be expressed as

$$E(\text{MgZn}_2|\text{Mg}^{2+}, \text{Zn}^{2+}) = \frac{1}{6e} [\mu(\text{Mg}^{2+}) + 2\mu(\text{Zn}^{2+}) - \mu_{\text{MgZn}_2}^{\text{bulk}}] \quad (2)$$

Since the chemical potential of some intermetallics are difficult to measure experimentally, we approximately express that of MgZn₂ in the form of enthalpy of formation by ignoring the influence of entropy

$$\mu_{\text{MgZn}_2}^{\text{bulk}} = \mu_{\text{Mg}} + 2\mu_{\text{Zn}} \approx \mu_{\text{Mg}}^{\text{bulk}} + 2\mu_{\text{Zn}}^{\text{bulk}} + \Delta H_{\text{MgZn}_2}^{\text{bulk}} \quad (3)$$

where μ_{Mg} and μ_{Zn} are the chemical potential of Mg and Zn atoms in MgZn₂, $\mu_{\text{Mg}}^{\text{bulk}}$ and $\mu_{\text{Zn}}^{\text{bulk}}$ are the chemical potentials of Mg and Zn in its standard elemental state (bulk hcp Mg and Zn), respectively. $\Delta H_{\text{MgZn}_2}^{\text{bulk}}$ is the enthalpy of formation of MgZn₂, which is taken from Material Project database [56]. The calculated equilibrium potential of MgZn₂ is −1.41 V_{SHE}, higher than that of Mg, indicating MgZn₂ will act as cathode in the galvanic reaction of Mg-Zn alloys.

It has previously been observed that the corrosion potential is strongly related to work function [57–59], we further compared the work function of Mg and MgZn₂. The calculated work function of MgZn₂ with the favored surface termination is 3.88 eV, larger than that of Mg (0001), 3.70 eV. This means it will need more energy to lose an electron for MgZn₂ than Mg, and thus MgZn₂ will serve as local cathode during the corrosion, in agreement with our equilibrium potential results.

3.2. Surface energy of MgZn₂

To investigate the water decomposition and hydrogen evolution process on MgZn₂ surfaces, we firstly determined its most stable surface termination based on the surface energy (γ). The chemical potential of Mg and Zn atoms in MgZn₂, μ_{Mg} and μ_{Zn} , shall be less than that of the corresponding elemental solid state [60,61] to avoid the precipitation of solid metals and satisfy the following equations

$$\mu_{\text{Mg}} < \mu_{\text{Mg}}^{\text{bulk}} \quad (4)$$

$$\mu_{\text{Zn}} < \mu_{\text{Zn}}^{\text{bulk}} \quad (5)$$

Combining Eq. (3), Eq. (4) and Eq. (5), we can obtain the allowed atomic chemical potentials in MgZn₂, as shown below

$$\mu_{\text{Mg}}^{\text{bulk}} + \Delta H_{\text{MgZn}_2}^{\text{bulk}} < \mu_{\text{Mg}} < \mu_{\text{Mg}}^{\text{bulk}} \quad (6)$$

$$\mu_{\text{Zn}}^{\text{bulk}} + \frac{1}{2}\Delta H_{\text{MgZn}_2}^{\text{bulk}} < \mu_{\text{Zn}} < \mu_{\text{Zn}}^{\text{bulk}} \quad (7)$$

The calculated surface energies of MgZn₂ shown in Fig. 1 indicate that under Zn-rich condition, (0001)-Zn^{II} surface is most stable, while under Mg-rich condition, (0001)-Mg^{II} surface of MgZn₂ has the lowest surface energy, the configuration of which is shown in Fig. 2. Considering a Mg-rich condition shall be achieved in the Mg alloys. Thus, (0001)-Mg^{II} surface of MgZn₂ is most likely to be present and would be further considered for the cathodic reactions in section 3.3.

3.3. Cathodic reaction on MgZn₂

The cathodic reaction on MgZn₂ is



One of the main products of cathodic reaction during the corrosion process is H₂. From the mechanism of HER, there are three basic reactions, namely, the Volmer reaction, the Tafel reaction and the Heyrovsky reaction [62]. In a neutral solution, we consider the HER on metal surface follows the Volmer-Tafel mechanism [63,64], which includes water dissociation, hydrogen ion discharge and diffusion, and further recombination of H adatoms (H*). Hence, to study the galvanic corrosion of Mg-Zn binary alloys, we should first examine the adsorption and decomposition of H₂O molecules on MgZn₂ surface in details.

The adsorption energy (E_{ads}) is calculated to represent the system stability after adsorbing related molecular or atomic species, which is calculated by

$$E_{\text{ads}}^{\text{H}} = E_{\text{slab}^*\text{H}} - E_{\text{slab}} - \frac{1}{2}E_{\text{H}_2} \quad (9)$$

where $E_{\text{slab}^*\text{H}}$ is the total energy of the slab with one H* on the surface. Similarly, we also calculated the adsorption energy (E_{ads}) of OH, H₂ and H₂O, namely $E_{\text{ads}}^{\text{OH}}$, $E_{\text{ads}}^{\text{H}_2}$, and $E_{\text{ads}}^{\text{H}_2\text{O}}$.

As shown in Fig. 2, we selected representative top, hollow, and bridge initial adsorption sites for H and OH on (0001)-Mg^{II} surface, and the adsorption energies are listed in Table 1. After structure optimization, it is found that the most stable adsorption site for H* atom is between the first layer Mg (denoted as Mg^I) and Zn atom with the adsorption energy of 0.04 eV. While OH* prefers the site enclosed by second layer Mg atom (denoted as Mg²), Mg^I and Zn atom with the adsorption energy of -1.19 eV. It is interesting that after the structure optimization, OH*, which is initially located at B1, B2, TMg² and TZn initial site, will move to same stable site according to the symmetry, causing the small adsorption energy difference. The details about the

most stable adsorption sites of H* and OH* are shown in Fig. S2.

As for water adsorption, we consider 15 possible initial configurations (shown in Fig. S3). After structure optimization, the water molecule at TMg¹-II site (O atom on the top site of first layer Mg and the center of two H atoms point to second layer Mg) possesses the lowest adsorption energy of -0.60 eV, indicating the water adsorption process is exothermic and thermodynamically favorable. The NEB calculations were performed further to obtain the minimum energy path (MEP) for the water dissociation reaction. The final state was determined to be the lowest adsorption energy state of H* and OH* co-adsorption.

Fig. 3(a) shows the MEP for the dissociation of H₂O* on the MgZn₂ surface with a reaction barrier of 0.53 eV. The final state with adsorbed H* and OH* on MgZn₂ surface is 0.69 eV lower than the initial adsorbed H₂O* state, enabling the dissociation reaction to easily proceed thermodynamically. Moreover, the relative energy change during the hydrogen atom diffusion and HER process are also investigated as shown in Fig. 3(b) and Fig. 3(c). For both processes, the energy differences between the initial and final state are negligible (0 and 0.04 eV). The energy barriers for the hydrogen atom diffusion and hydrogen evolution are 0.12 eV and 0.90 eV, respectively.

To better understand the cathodic reaction on MgZn₂, a schematic reaction path of the HER on MgZn₂ (0001)-Mg^{II} surface containing four sequential steps, namely water adsorption, water dissociation, hydrogen atom diffusion and recombination, was summarized in Fig. 4. According to Arrhenius equation and transition state theory, the relative value of reaction barrier can be compared in order to estimate the rate-limiting step of the whole reaction. The water absorption and dissociation step correspond to red line of Fig. 4. One water molecule first adsorbs with its oxygen atom at the TMg¹-II site, releasing the energy of 0.60 eV. Subsequently, water molecule undergoes dissociation along with hydrogen atom and hydroxide moving towards B3 and B2 site, respectively. The energy barrier of water dissociation is 0.53 eV and the energy of hydrogen atom and hydroxide co-adsorption is lower than water molecule adsorption, which implies water dissociation is a thermodynamically favored process. The third step is presented in green color of Fig. 4. Without considering hydroxide, the adsorption energy of a single hydrogen atom is 0.04 eV and the reaction barrier for hydrogen atom diffusion from B3 site to adjacent B3 site is 0.12 eV. Finally, the hydrogen atom recombination was shown in blue color. With increasing the H atom coverage, the adsorption energy will slightly decrease. Two adjacent H atom on B3 site will move to TMg¹ site to evolve hydrogen molecule gas with the barrier of 0.90 eV. Among the whole HER process, the hydrogen atom recombination process (Tafel process) with the largest reaction energy barrier is considered to be the rate-limiting step.

The cathodic reaction on MgZn₂ would be further compared to that of Mg-Ge series alloy (composed of Mg matrix and Mg₂Ge second phase [65]) and pure Mg. Previous studies on pure Mg and dilute Mg alloys have calculated that Tafel reaction is the rate-determining step during the HER process [64,66]. A similar trend was also observed in this study on MgZn₂ surface as shown in Fig. 5(a). However, water decomposition possesses the largest activation energy barrier on Mg₂Ge, which is believed as a result of highly positive adsorption energy of H*. Nørskov fitted the relationship between exchange current density and free energy of H* (ΔG_{H^*}) [67] (also known as volcano curve). If ΔG_{H^*} is highly negative, H* will be strongly adsorbed on the surface and subsequent Tafel step will be hindered. Inversely, a highly positive ΔG_{H^*} value, like Mg₂Ge surface, will give rise to a slow rate for entire reaction because of repulsive interactions between the proton and cathode surface. Thus, a corrosion resistant Mg intermetallics are expected to have a large $|\Delta G_{\text{H}^*}|$. Fig. 5 (b) shows ΔG_{H^*} on three surfaces and each of them is above zero. The strong repulsive interaction caused by large ΔG_{H^*} on Mg₂Ge surface leads to a negligible Tafel reaction barrier. More specifically, the experimental results validate the relationship between corrosion rate and ΔG_{H^*} . The corrosion current density of Mg-Zn and Mg-Ge alloy is 23 to 52 $\mu\text{A}/\text{cm}^2$ and 0.7 to 35.6 $\mu\text{A}/\text{cm}^2$, respectively,

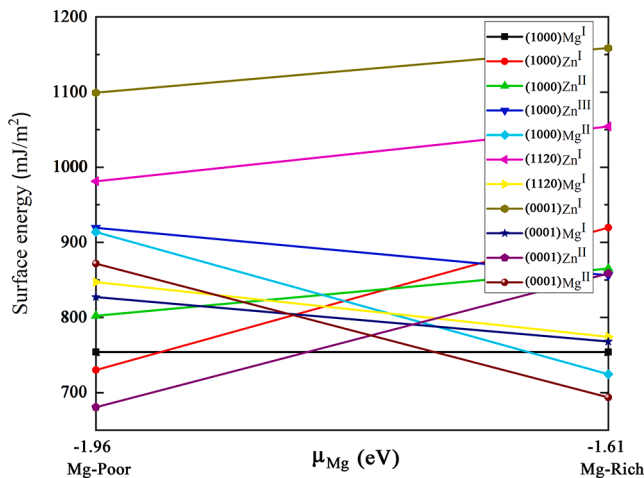


Fig. 1. The calculated surface energy of the different surface terminations of MgZn₂ as a function of the chemical potentials of Mg, μ_{Mg} .

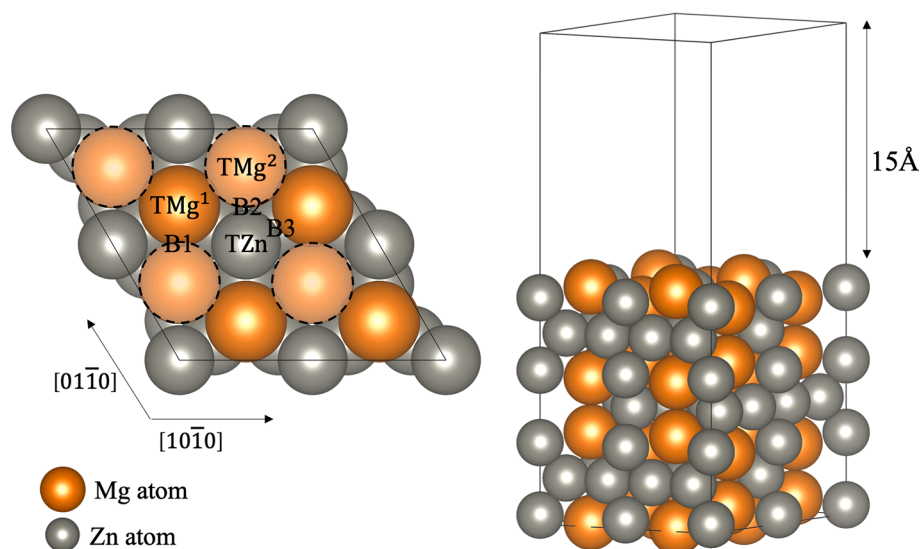


Fig. 2. Schematic top and side views of the MgZn_2 (0001)- Mg^{II} surface with the adsorption sites: T (top), B (bridge), H (hollow). The orange atoms represent first layer Mg atoms (denoted by Mg^1), the light orange atoms in dashed circle represent the second layer Mg atoms (denoted by Mg^2). TZn, TMg^1 , and TMg^2 represent the top sites over Zn atoms, first/second layer Mg^1/Mg^2 atoms. B1, B2, and B3 represent the Bridge sites between Mg^1 and Mg^2 , Zn and Mg^2 , Mg^1 and Zn, respectively.

Table 1

The adsorption energy (E_{ads}) of H^* and OH^* at different initial adsorption sites on MgZn_2 (0001)- Mg^{II} surface with the lowest E_{ads} shown in bold. Some E_{ads} are close since the adsorbate moves to same location after structural optimization.

Initial adsorption sites	E_{ads} (eV)					
	B1	B2	B3	TMg^1	TMg^2	TZn
H	0.04	0.16	0.04	0.67	0.74	0.29
OH	-1.18	-1.19	-0.89	-0.27	-1.19	-1.18

depending on the content of alloying elements [68,69]. The corrosion current density of pure Mg is about $680 \mu\text{A}/\text{cm}^2$, indicating it suffers the largest corrosion rate compared with Mg-Zn and Mg-Ge series alloy [68]. Assuming the corrosion under the same anodic reaction and ignoring the influence of solute elements, we found the larger $|\Delta G_{\text{H}^*}|$ corresponds to a smaller corrosion current density, which may be caused by weak or strong interaction during the proton adsorption(desorption) process. This could be a simple and quick criterion for screening the promising corrosion resistant Mg intermetallics.

Further calculations on the kinetic barriers of HER on different Mg intermetallics are needed to screen the promising intermetallic

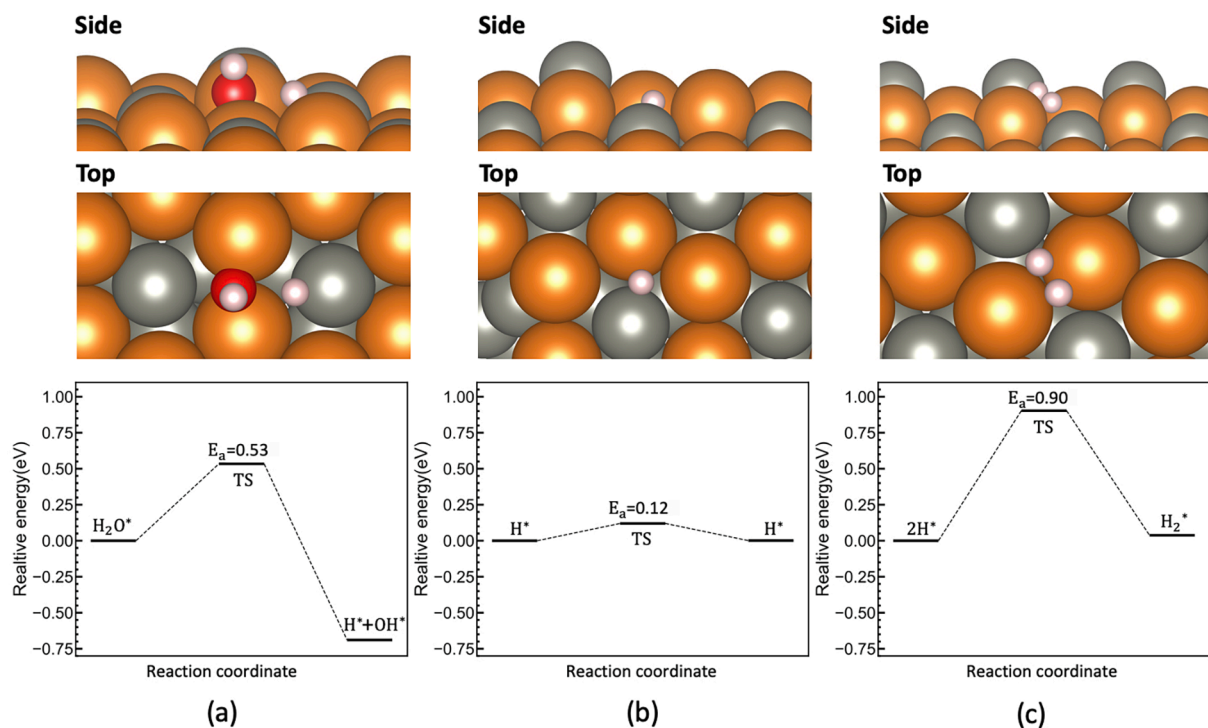


Fig. 3. Optimized geometries (side and top view, upper panel) of reaction transition states (TS) and relative energy change (lower panel) for the water decomposition, H adatom diffusion and hydrogen evolution reaction on the MgZn_2 (0001)- Mg^{II} surface.

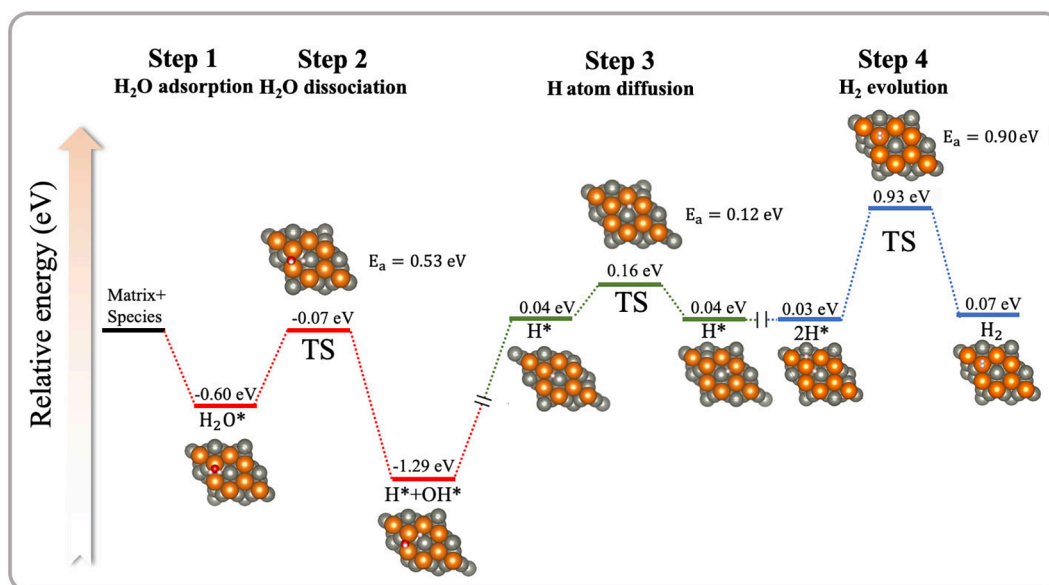


Fig. 4. Energy diagram for water dissociation and subsequent hydrogen evolution reaction on MgZn₂ (0001)-Mg^{II} surface. The red, green and blue color represents water dissociation, H atom diffusion and hydrogen evolution reaction, respectively. Intermediate steps in the reaction are labeled with their respective chemistries, while transition states are labeled with TS.

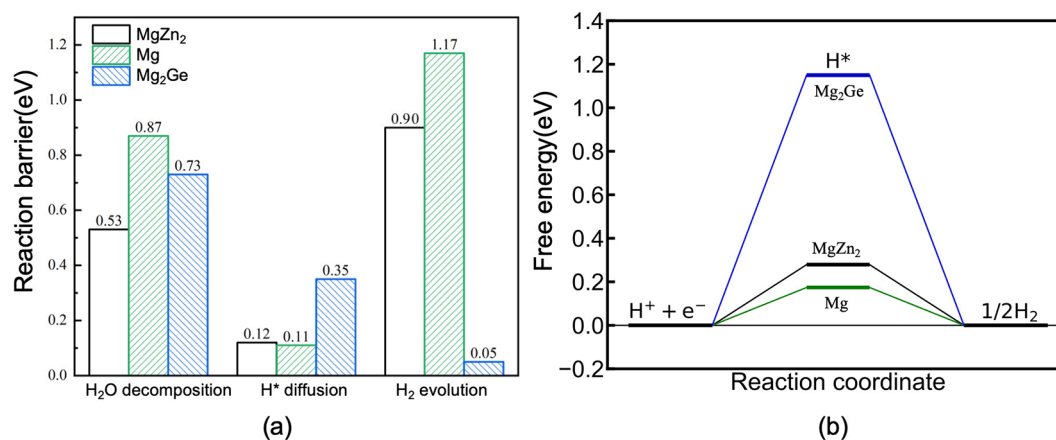


Fig. 5. (a) The activation energy barrier for water decomposition, H atom diffusion and hydrogen evolution. The reaction barriers of Mg and Mg₂Ge are summarized from literature [52,64,70]. (b) Calculated Gibbs free energies of hydrogen adsorption (ΔG_{H^*}) for Mg₂Ge, MgZn₂ and pure Mg. ΔG_{H^*} was calculated as $\Delta G_{H^*} = E_{ads}^H + \Delta E_{ZPE} - T\Delta S_H$, where $\Delta E_{ZPE} - T\Delta S_H$ is taken as 0.24 eV [67].

candidates. Additionally, the effect of dilute alloying additions on the anodic reaction (metal dissolution) reaction should not be neglected. Moreover, the formation of oxide layer, e.g. MgO or Mg(OH)₂, and the influence from the solution and other ions are beyond the scope of this study and would be investigated in the future.

4. Conclusion

In summary, we performed first-principles calculations to investigate the full hydrogen evolution reaction on MgZn₂ surface. Based on Volmer-Tafel mechanism, this process is typically divided into four steps: water adsorption, water dissociation, H* diffusion and hydrogen evolution. Moreover, the cathodic reaction activation energy barriers of MgZn₂, Mg₂Ge and Mg are compared. The conclusions can be summarized as following

- (a) Equilibrium potential could determine the nobility of phases. In the Mg-Zn alloys, the thermodynamic driving force of corrosion is the equilibrium potential difference between Mg matrix and

intermetallic phase, which causes dissolution of the Mg matrix. MgZn₂ intermetallic phase serves as the local cathode during the galvanic corrosion process.

- (b) By using NEB method, the pathway and reaction energy barriers for H₂O molecules decomposition, 0.53 eV, H atom diffusion, 0.12 eV and H₂ molecules evolution, 0.90 eV, were obtained, indicating the Tafel process is the rate-determining step during the cathodic reaction.
- (c) Free energy of H* (ΔG_{H^*}) is a quick criterion for screening the promising corrosion resistant Mg alloys. Too strong or too weak interaction between H* and surface contributes to a small corrosion current density.

CRediT authorship contribution statement

Yaowei Wang: Conceptualization, Methodology, Software, Formal analysis, Writing - original draft. **Tian Xie:** Conceptualization, Methodology. **Zhe Luo:** Conceptualization, Methodology. **Hong Zhu:** Supervision. **Xiaoqin Zeng:** Supervision.

Declaration of Competing Interest

The authors declare that they have no known competing financial interests or personal relationships that could have appeared to influence the work reported in this paper.

Acknowledgment

The research was financially supported by the National Key Research and Development Program of China, China (No. 2017YFB0701500 and No. 2016YFB0701202) and the National Natural Science Foundation of China, China (General Program No. 51474149). First-principles calculations were carried out with computational resources from Shanghai Jiao Tong University Super Computer Center. H. Zhu also thanks to the financial support from the University of Michigan (U-M) and Shanghai Jiao Tong University (SJTU) joint funding, China (AE604401) and Science and Technology Commission of Shanghai Municipality (No. 18511109302).

Appendix A. Supplementary data

Supplementary data to this article can be found online at <https://doi.org/10.1016/j.commatsci.2021.110532>.

References

- [1] M. Meinshausen, N. Meinshausen, W. Hare, S.C.B. Raper, K. Frieler, R. Knutti, D. J. Frame, M.R. Allen, Greenhouse-gas emission targets for limiting global warming to 2 °C, *Nature*. 458 (2009) 1158–1162, <https://doi.org/10.1038/nature08017>.
- [2] J.C. Fyfe, G.A. Meehl, M.H. England, M.E. Mann, B.D. Santer, G.M. Flato, E. d. Hawkins, N.P. Gillett, S.-P. Xie, Y. u. Kosaka, N.C. Swart, Making sense of the early-2000s warming slowdown, *Nat. Clim. Change*. 6 (3) (2016) 224–228, <https://doi.org/10.1038/nclimate2938>.
- [3] F. Cao, G.L. Song, A. Atrens, Corrosion and passivation of magnesium alloys, 2016. <https://doi.org/10.1016/j.corsci.2016.05.041>.
- [4] M. Esmaily, J.E. Svensson, S. Fajardo, N. Birbilis, G.S. Frankel, S. Virtanen, R. Arrabal, S. Thomas, L.G. Johansson, Fundamentals and advances in magnesium alloy corrosion, *Prog. Mater. Sci.* 89 (2017) 92–193, <https://doi.org/10.1016/j.pmatsci.2017.04.011>.
- [5] L.J. Liu, M. Schlesinger, Corrosion of magnesium and its alloys, *Corros. Sci.* 51 (8) (2009) 1733–1737, <https://doi.org/10.1016/j.corsci.2009.04.025>.
- [6] G.L. Makar, J. Kruger, Corrosion of magnesium, (n.d.) 16.
- [7] G.L. Song, A. Atrens, Corrosion mechanisms of magnesium alloys, *Adv Eng Mater.* 1 (1999) 11–33, [https://doi.org/10.1002/\(SICI\)1527-2648\(199909\)1:1<11::AID-ADEM11>3.0.CO;2-N](https://doi.org/10.1002/(SICI)1527-2648(199909)1:1<11::AID-ADEM11>3.0.CO;2-N).
- [8] S. Thomas, N.V. Medhekar, G.S. Frankel, N. Birbilis, Corrosion mechanism and hydrogen evolution on Mg, *Curr. Opin. Solid State Mater. Sci.* 19 (2) (2015) 85–94, <https://doi.org/10.1016/j.cossms.2014.09.005>.
- [9] A. Dobkowska, B. Adamczyk-Cieślak, A. Towarek, P. Maj, E. Ura-Bińczyk, M. Momeni, D. Kuc, E. Hadasik, J. Mizera, The Influence of Microstructure on Corrosion Resistance of Mg-3Al-1Zn-15Li (LAZ1531) Alloy, *J. Mater. Eng. Perform.* 29 (4) (2020) 2679–2686, <https://doi.org/10.1007/s11665-020-04775-0>.
- [10] M.A. Jingling, W. Jiuba, L.I. Gengxin, X.V. Chunhua, The corrosion behaviour of Al-Zn-In-Mg-Ti alloy in NaCl solution, *Corros. Sci.* 52 (2) (2010) 534–539, <https://doi.org/10.1016/j.corsci.2009.10.010>.
- [11] N. El-Mahallawy, H. Palkowski, A. Klingner, A. Dīaa, M. Shoeib, Effect of 1.0 wt. % Zn addition on the microstructure, mechanical properties, and bio-corrosion behaviour of micro alloyed Mg-0.24Sn-0.04Mn alloy as biodegradable material, *Mater. Today Commun.* 24 (2020) 100999, <https://doi.org/10.1016/j.mtcomm.2020.100999>.
- [12] K. Gusieva, C.H.J. Davies, J.R. Scully, N. Birbilis, Corrosion of magnesium alloys: the role of alloying, *Int. Mater. Rev.* 60 (3) (2015) 169–194, <https://doi.org/10.1179/1743280414Y.0000000046>.
- [13] Y. Li, C. Wen, D. Mushahary, R. Sravanthi, N. Harishankar, G. Pande, P. Hodgson, Mg-Zr-Sr alloys as biodegradable implant materials, *Acta Biomater.* 8 (8) (2012) 3177–3188, <https://doi.org/10.1016/j.actbio.2012.04.028>.
- [14] W. Liu, F. Cao, L. Zhong, L. Zheng, B. Jia, Z. Zhang, J. Zhang, Influence of rare earth element Ce and La addition on corrosion behavior of AZ91 magnesium alloy: Influence of Ce and La on the corrosion of AZ91, *Mater. Corros.* 60 (10) (2009) 795–803, <https://doi.org/10.1002/maco.200805179>.
- [15] Y.u. Fan, G. Wu, C. Zhai, Influence of cerium on the microstructure, mechanical properties and corrosion resistance of magnesium alloy, *Mater. Sci. Eng. A*. 433 (1–2) (2006) 208–215, <https://doi.org/10.1016/j.msea.2006.06.109>.
- [16] F. Rosalbino, E. Angelini, S. De Negri, A. Saccone, S. Delfino, Effect of erbium addition on the corrosion behaviour of Mg–Al alloys, *Intermetallics*. 13 (1) (2005) 55–60, <https://doi.org/10.1016/j.intermet.2004.05.007>.
- [17] Kubásek, Dvorský, Sedý, Msallamová, Levorová, Foltán, Vojtěch, Sedý, Msallamová, Levorová, Foltán, Vojtěch, The Fundamental Comparison of Zn–2Mg and Mg–4Y–3RE Alloys as a Perspective Biodegradable Materials, *Materials*. 12 (22) (2019) 3745, <https://doi.org/10.3390/ma12223745>.
- [18] E. Zhang, D. Yin, L. Xu, L. Yang, K.e. Yang, Microstructure, mechanical and corrosion properties and biocompatibility of Mg–Zn–Mn alloys for biomedical application, *Mater. Sci. Eng. C*. 29 (3) (2009) 987–993, <https://doi.org/10.1016/j.msec.2008.08.024>.
- [19] H.R. Bakhsheshi-Rad, E. Hamzah, A. Fereidouni-Lotfabad, M. Daroonparvar, M.A. M. Yajid, M. Mezbahul-Islam, M. Kasiri-Asgarani, M. Medraj, Microstructure and bio-corrosion behavior of Mg-Zn and Mg-Zn-Ca alloys for biomedical applications: Microstructure and bio-corrosion behavior of Mg-Zn and Mg-Zn-Ca alloys, *Mater. Corros.* 65 (12) (2014) 1178–1187, <https://doi.org/10.1002/maco.v65.1210.1002/maco.201307588>.
- [20] Q. Xiang, R.Z. Wu, M.L. Zhang, Influence of Sn on microstructure and mechanical properties of Mg–5Li–3Al–2Zn alloys, *J. Alloys Compd.* 477 (1–2) (2009) 832–835, <https://doi.org/10.1016/j.jallcom.2008.10.166>.
- [21] Y. Guangyin, L. Manping, D. Wenjiang, A. Inoue, Microstructure and mechanical properties of Mg–Zn–Si-based alloys, *Mater. Sci. Eng. A*. 357 (1–2) (2003) 314–320, [https://doi.org/10.1016/S0921-5093\(03\)00208-9](https://doi.org/10.1016/S0921-5093(03)00208-9).
- [22] J. Han, K. Ogle, Editors' Choice—Dealloying of MgZn₂ Intermetallic in Slightly Alkaline Chloride Electrolyte and Its Significance in Corrosion Resistance, *J. Electrochem. Soc.* 164 (14) (2017) C952–C961, <https://doi.org/10.1149/2.0341714jes>.
- [23] L.Y. Wei, G.L. Dunlop, H. Westengen, Precipitation hardening of Mg-Zn and Mg-Zn-RE alloys, *Metall. Mater. Trans. A*. 26 (7) (1995) 1705–1716.
- [24] Y. Liu, G. Yuan, C. Lu, W. Ding, Stable icosahedral phase in Mg–Zn–Gd alloy, *Scr. Mater.* 55 (10) (2006) 919–922, <https://doi.org/10.1016/j.scriptamat.2006.07.035>.
- [25] C.L. Mendis, K. Oh-ishi, K. Hono, Enhanced age hardening in a Mg–2.4at.% Zn alloy by trace additions of Ag and Ca, *Scr. Mater.* 57 (6) (2007) 485–488, <https://doi.org/10.1016/j.scriptamat.2007.05.031>.
- [26] C. Mendis, K. Ohishi, Y. Kawamura, T. Honma, S. Kamado, K. Hono, Precipitation-hardenable Mg–2.4Zn–0.1Ag–0.1Ca–0.16Zr (at.%) wrought magnesium alloy, *Acta Mater.* 57 (3) (2009) 749–760, <https://doi.org/10.1016/j.actamat.2008.10.033>.
- [27] C. Yao, Z. Wang, S.L. Tay, T. Zhu, W. Gao, Effects of Mg on microstructure and corrosion properties of Zn–Mg alloy, *J. Alloys Compd.* 602 (2014) 101–107, <https://doi.org/10.1016/j.jallcom.2014.03.025>.
- [28] S. Zhang, X. Zhang, C. Zhao, J. Li, Y. Song, C. Xie, H. Tao, Y. Zhang, Y. He, Y. Jiang, Y. Bian, Research on an Mg–Zn alloy as a degradable biomaterial, *Acta Biomater.* 6 (2010) 626–640, <https://doi.org/10.1016/j.actbio.2009.06.028>.
- [29] N. Birbilis, R.G. Buchheit, Electrochemical Characteristics of Intermetallic Phases in Aluminum Alloys, *J. Electrochem. Soc.* 152 (4) (2005) B140, <https://doi.org/10.1149/1.1869984>.
- [30] L. Shao, T.-T. Shi, J. Zheng, H.-C. Wang, X.-Z. Pan, B.-Y. Tang, First-principles study of point defects in C14 MgZn₂ Laves phase, *J. Alloys Compd.* 654 (2016) 475–481, <https://doi.org/10.1016/j.jallcom.2015.09.142>.
- [31] P. Mao, B.o. Yu, Z. Liu, F. Wang, Y. Ju, First-principles calculations of structural, elastic and electronic properties of AB₂ type intermetallics in Mg–Zn–Ca–Cu alloy, *J. Magnes. Alloys*. 1 (3) (2013) 256–262, <https://doi.org/10.1016/j.jma.2013.10.001>.
- [32] M.-M. Wu, L.I. Wen, B.-Y. Tang, L.-M. Peng, W.-J. Ding, First-principles study of elastic and electronic properties of MgZn₂ and ScZn₂ phases in Mg–Sc–Zn alloy, *J. Alloys Compd.* 506 (1) (2010) 412–417, <https://doi.org/10.1016/j.jallcom.2010.07.018>.
- [33] T. Tsuru, M. Yamaguchi, K. Ebihara, M. Itakura, Y. Shihara, K. Matsuda, H. Toda, First-principles study of hydrogen segregation at the MgZn₂ precipitate in Al-Mg-Zn alloys, *Comput. Mater. Sci.* 148 (2018) 301–306, <https://doi.org/10.1016/j.commatsci.2018.03.009>.
- [34] A.D. Gabbardo, G.S. Frankel, Hydrogen evolution on bare Mg surfaces using the scratched electrode technique, *Corros. Sci.* 164 (2020) 108321, <https://doi.org/10.1016/j.corsci.2019.108321>.
- [35] Z.W. Wang, X.J. Guo, W. Yuan, Z.Y. Ding, First-Principles Study of Hydrogen Atom Diffusion on Transition Metal Doped Mg(0001) Surface, *Adv. Mater. Res.* 873 (2013) 101–109, <https://doi.org/10.4028/www.scientific.net/AMR.873.101>.
- [36] H. Lei, C. Wang, Y. Yao, Y. Wang, M. Hupaló, D. McDougall, M. Tringides, K. Ho, Strain effect on the adsorption, diffusion, and molecular dissociation of hydrogen on Mg (0001) surface, *J. Chem. Phys.* 139 (22) (2013) 224702, <https://doi.org/10.1063/1.4839595>.
- [37] M. Chen, Z.-Z. Cai, X.-B. Yang, M. Zhu, Y.-J. Zhao, Theoretical study of hydrogen dissociation and diffusion on Nb and Ni co-doped Mg(0001): A synergistic effect, *Surf. Sci.* 606 (13–14) (2012) L45–L49, <https://doi.org/10.1016/j.susc.2012.03.008>.
- [38] G. Wu, J. Zhang, Y. Wu, Q. Li, K. Chou, X. Bao, Hydrogenation mechanism in lanthanum-activated magnesium films, *Appl. Phys. A*. 102 (3) (2011) 739–745, <https://doi.org/10.1007/s00339-010-5976-6>.
- [39] A.J. Du, S.C. Smith, X.D. Yao, G.Q. Lu, First-Principle Study of Adsorption of Hydrogen on Ti-Doped Mg(0001) Surface, *J. Phys. Chem. B*. 110 (43) (2006) 21747–21750, <https://doi.org/10.1021/jp063286o>.
- [40] S. Banerjee, C.G.S. Pillai, C. Majumder, First-principles study of the H₂ interaction with transition metal (Ti, V, Ni) doped Mg(0001) surface: Implications for H-storage materials, *J. Chem. Phys.* 129 (17) (2008) 174703, <https://doi.org/10.1063/1.3000673>.
- [41] A.D. Südholz, N.T. Kirkland, R.G. Buchheit, N. Birbilis, Electrochemical Properties of Intermetallic Phases and Common Impurity Elements in Magnesium Alloys, *Electrochem. Solid-State Lett.* 14 (2) (2011) C5, <https://doi.org/10.1149/1.3523229>.

- [42] D. Sholl, J.A. Steckel, *Density Functional Theory: A Practical Introduction*, John Wiley & Sons, 2011.
- [43] P.E. Blöchl, Projector augmented-wave method, *Phys. Rev. B* 50 (24) (1994) 17953–17979, <https://doi.org/10.1103/PhysRevB.50.17953>.
- [44] J. Hafner, Ab-initio simulations of materials using VASP: Density-functional theory and beyond, *J. Comput. Chem.* 29 (2008) 2044–2078.
- [45] W. Kohn, L.J. Sham, Self-Consistent Equations Including Exchange and Correlation Effects, *Phys. Rev.* 140 (4A) (1965) A1133–A1138, <https://doi.org/10.1103/PhysRev.140.A1133>.
- [46] J.P. Perdew, W. Yue, Accurate and simple density functional for the electronic exchange energy: Generalized gradient approximation, *Phys. Rev. B* 33 (1986) 8800.
- [47] X. Gao, J.F. Nie, Characterization of strengthening precipitate phases in a Mg–Zn alloy, *Scr. Mater.* 56 (8) (2007) 645–648, <https://doi.org/10.1016/j.scriptamat.2007.01.006>.
- [48] J.S. Chun, J.G. Byrne, Precipitate strengthening mechanisms in magnesium zinc alloy single crystals, *J. Mater. Sci.* 4 (10) (1969) 861–872.
- [49] D. Andrae, B. Paulus, U. Wedig, M. Jansen, A First-Principles Study of Electronic Structure of the Laves Phase MgZn₂, *Z. Für Anorg. Allg. Chem.* 639 (11) (2013) 1963–1967, <https://doi.org/10.1002/zaac.v639.1110.1002/zaac.201300023>.
- [50] Z. Shi, J.X. Jia, A. Atrens, Galvanostatic anodic polarization curves and galvanic corrosion of high purity Mg in 3.5% NaCl saturated with Mg(OH)₂, *Corros. Sci.* 60 (2012) 296–308.
- [51] G. Song, B. Johannesson, S. Hapugoda, D. StJohn, Galvanic corrosion of magnesium alloy AZ91D in contact with an aluminium alloy, steel and zinc, *Corros. Sci.* 46 (4) (2004) 955–977.
- [52] Z. Luo, J. Xu, Y. Wang, T. Xie, H. Zhu, T. Ying, D. Li, L. Wang, X. Zeng, C. Wolverton, W. Ding, Theoretical Analysis of the Galvanic Corrosion Behavior of Mg-Ge Binary Alloy, *J. Electrochem. Soc.* 166 (13) (2019) C421–C427, <https://doi.org/10.1149/2.1061913jes>.
- [53] E. McCafferty (Ed.), *Introduction to Corrosion Science*, Springer New York, New York, NY, 2010.
- [54] K.A. Persson, B. Waldwick, P. Lazić, G. Ceder, Prediction of solid-aqueous equilibria: Scheme to combine first-principles calculations of solids with experimental aqueous states, *Phys Rev B - Condens Matter Mater Phys.* 85 (2012) 1–12, <https://doi.org/10.1103/PhysRevB.85.235438>.
- [55] S.P. Ong, S. Cholia, A. Jain, M. Brafman, D. Gunter, G. Ceder, K.A. Persson, The Materials Application Programming Interface (API): A simple, flexible and efficient API for materials data based on REpresentational State Transfer (REST) principles, *Comput. Mater. Sci.* 97 (2015) 209–215, <https://doi.org/10.1016/j.commatsci.2014.10.037>.
- [56] A. Jain, S.P. Ong, G. Hautier, W. Chen, W.D. Richards, S. Dacek, S. Cholia, D. Gunter, D. Skinner, G. Ceder, K.A. Persson, Commentary: The Materials Project: A materials genome approach to accelerating materials innovation, *APL Mater.* 1 (1) (2013) 011002, <https://doi.org/10.1063/1.4812323>.
- [57] Y. Jin, M. Liu, C. Zhang, C. Leygraf, L. Wen, J. Pan, First-principle calculation of Volta potential of intermetallic particles in aluminum alloys and practical implications, *J. Electrochem. Soc.* 164 (9) (2017) C465–C473.
- [58] M.F. Hurley, C.M. Efav, P.H. Davis, J.R. Croteau, E. Graugnard, N. Birbilis, Volta potentials measured by scanning Kelvin probe force microscopy as relevant to corrosion of magnesium alloys, *Corrosion* 71 (2) (2015) 160–170.
- [59] H. Ma, X.-Q. Chen, R. Li, S. Wang, J. Dong, W. Ke, First-principles modeling of anisotropic anodic dissolution of metals and alloys in corrosive environments, *Acta Mater.* 130 (2017) 137–146, <https://doi.org/10.1016/j.actamat.2017.03.027>.
- [60] Z. Alahmed, H. Fu, First-principles determination of chemical potentials and vacancy formation energies in Pb Ti O₃ and Ba Ti O₃, *Phys. Rev. B* 76 (2007), 224101, <https://doi.org/10.1103/PhysRevB.76.224101>.
- [61] Doping asymmetry in wide-bandgap semiconductors: Origins and solutions - Yan - 2008 - physica status solidi (b) - Wiley Online Library, (n.d.). <https://onlinelibrary.wiley.com/doi/abs/10.1002/pssb.200743334> (accessed September 4, 2019).
- [62] H. Ma, L. Wu, C. Liu, M. Liu, C. Wang, D. Li, X.-Q. Chen, J. Dong, W. Ke, First-principles modeling of the hydrogen evolution reaction and its application in electrochemical corrosion of Mg, *Acta Mater.* 183 (2020) 377–389, <https://doi.org/10.1016/j.actamat.2019.11.025>.
- [63] S. Sharifi-Asl, D.D. Macdonald, Investigation of the Kinetics and Mechanism of the Hydrogen Evolution Reaction on Copper, *J. Electrochem. Soc.* 160 (6) (2013) H382–H391, <https://doi.org/10.1149/2.143306jes>.
- [64] K.S. Williams, V. Rodriguez-Santiago, J.W. Andzelm, Modeling reaction pathways for hydrogen evolution and water dissociation on magnesium, *Electrochimica Acta* 210 (2016) 261–270, <https://doi.org/10.1016/j.electacta.2016.04.128>.
- [65] R.L. Liu, M.F. Hurley, A. Kvryan, G. Williams, J.R. Scully, N. Birbilis, Controlling the corrosion and cathodic activation of magnesium via microalloying additions of Ge, *Sci. Rep.* 6 (2016) 28747, <https://doi.org/10.1038/srep28747>.
- [66] T. Vegge, Locating the rate-limiting step for the interaction of hydrogen with Mg (0001) using density-functional theory calculations and rate theory, *Phys. Rev. B* 70 (2004), 035412, <https://doi.org/10.1103/PhysRevB.70.035412>.
- [67] J.K. Nørskov, T. Bligaard, A. Logadottir, J.R. Kitchin, J.G. Chen, S. Pandalov, U. Stimming, Trends in the Exchange Current for Hydrogen Evolution, *J. Electrochem. Soc.* (n.d.) 4.
- [68] S. Cai, T. Lei, N. Li, F. Feng, Effects of Zn on microstructure, mechanical properties and corrosion behavior of Mg–Zn alloys, *Mater. Sci. Eng. C* 32 (8) (2012) 2570–2577, <https://doi.org/10.1016/j.msec.2012.07.042>.
- [69] D. Bian, W. Zhou, J. Deng, Y. Liu, W. Li, X. Chu, P. Xiu, H. Cai, Y. Kou, B. Jiang, Y. Zheng, Development of magnesium-based biodegradable metals with dietary trace element germanium as orthopaedic implant applications, *Acta Biomater.* 64 (2017) 421–436, <https://doi.org/10.1016/j.actbio.2017.10.004>.
- [70] M. Pozzo, D. Alfè, Hydrogen dissociation and diffusion on transition metal (=Ti, Zr, V, Fe, Ru Co, Rh, Ni, Pd, Cu, Ag)-doped Mg(0001) surfaces, *Int. J. Hydrog. Energy* 34 (4) (2009) 1922–1930, <https://doi.org/10.1016/j.ijhydene.2008.11.109>.